Fluidization of variable short fiber/powder mixtures: hydrodynamic investigation

CRediT authorship contribution statement

- 1st author: **Thomas DA CALVA MOUILLEVOIS**[1,2] (corresponding author): dacalva@lcts.u-bordeaux.fr, Conceptualization, Methodology, Formal analysis, Investigation, Writing - Original Draft, Writing - Review & Editing, Visualization.
- 2nd author: **Matthias AUDREN-PAUL**[3]: mapaul001@univ-pau.fr, Investigation.
- 3rd author: **Georges CHOLLON**[1]: chollon@lcts.u-bordeaux.fr, Writing - Review & Editing, Supervision, Project administration.
- 4th author: **Nathalie BERTRAND**[1,2]: bertrand@lcts.u-bordeaux.fr, Writing - Review & Editing, Supervision, Project administration.

[1] *ThermoStructural Composites Laboratory (LCTS), 3 Allée de la Boétie, 33600 Pessac, France*

[2] *University of Bordeaux, 351 Cour de la Libération, 33400 Talence, France*

[3] *National School of Chemical and Technological Engineering, 4 Allée Emile Monso, 31030 Toulouse, France*

Highlights

- Numerical determination of the minimum fluidization velocity as a function of the operating parameters
- Prediction of the equivalent hydraulic diameter of short fiber/powder mixtures in variable proportions
- Coefficient estimation of the Darcy-Klinkenberg hydrodynamic equation adapted to fiber/powder mixtures
- Accurate prediction (± 10%) of the minimum fluidization velocity by semi-empirical correlation with Kn
- Extension and specification of the fluidized bed expansion equation as a function of operating parameters

Graphical abstract

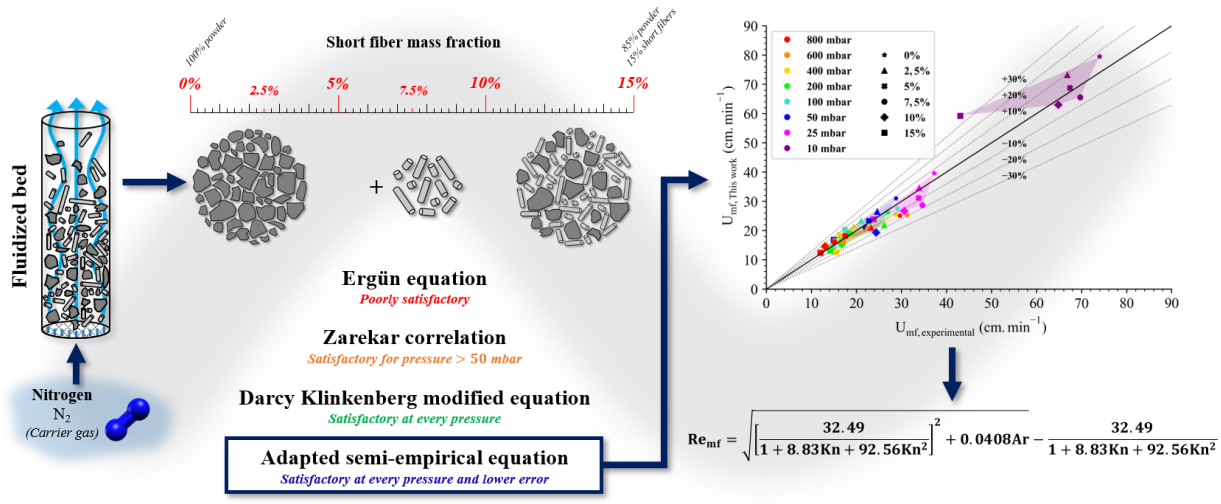

Colors for figures

For a proper readability of the figures, all require color printing.

Abstract

The behavior of a particle mixture composed of short fibers and silicon carbide powder in variable proportions has been experimentally investigated. The study shows that the hydrodynamic behavior of a bed initially composed of powder is affected as soon as a few percent of short fibers are added. The minimum fluidization velocity (U_{mf}) is globally lowered and the intrinsic properties of the porous medium (equivalent particle diameter, porosity, flow coefficients…) are altered. Several hydrodynamic equations describing U_{mf} as a function of the pressure are considered and the intrinsic properties of the bed such as the hydraulic diameter or the Darcy and Knudsen coefficients are fitted. The Darcy-Klinkenberg equation on one hand and a semi-empirical correlation based on Ergün's equation on the other hand, are both adapted to describe the U_{mf} behavior as a function of a limited number of initial parameters. The semi-empirical correlation leads to the best U_{mf} prediction, with an absolute error of less than 10%, using only the temperature, pressure and percentage of fibers in the mixture as input parameters.

Keywords

Fluidized bed, Minimum fluidization velocity, Hydrodynamic, Particle mixture, Short fibers

46

47 **Nomenclature**

A	Semi-empirical coefficient of Re(Ar) equation	(-)
a	Coefficient for the curve fitting of $\Psi_s d_g(\%_f)$	(-)
Ar	Archimedes number	(-)
B	Semi-empirical coefficient of Re(Ar) equation	(-)
b	Coefficient for the curve fitting of $\Psi_s d_g(\%_f)$	(-)
C_1	Constant coefficient for $1/(\Psi_s \varepsilon_{mf}^3)$	(-)
c	Gas molecular velocity	$(m.s^{-1})$
c_0	Adjustment factor for $K_2(Kn)$ equation	(-)
c_1	Adjustment factor for $K_2(Kn)$ equation	(-)
c_2	Adjustment factor for $K_2(Kn)$ equation	(-)
d_g	Average particle diameter	(m)
d_p	Pore diameter	(m)
d_{sv}	Surface volume diameter or Sauter diameter	(m)
d_{sv}^f	Surface volume diameter of the short fibers	(m)
d_{sv}^p	Surface volume diameter of the powder	(m)
D_K	Knudsen diffusion coefficient	$(m^2.s^{-1})$
g	Gravitational force constant	$(9.81\ m.s^{-2})$
H	Absolute bed height	(m)
H^*	Normalized bed height	(-)
H_{mf}	Bed height at minimum fluidization velocity	(m)
K	Permeability	(m^2)
K_1	Semi-empirical coefficient of Ar(Re) equation	(-)
K_2	Semi-empirical coefficient of Ar(Re) equation	(-)
K_B	Boltzmann constant	$(1.380649.10^{-23}\ m^2.kg.s^{-2}.K^{-1})$
Kn	Knudsen number	(-)
k_2	Inertial flow coefficient	(-)
m	Bed mass	(kg)
M	Molar mass	$(kg.mol^{-1})$
n	Coefficient for the curve fitting of $\Psi_s d_g(\%_f)$	(-)
n_1	Bed expansion equation factor for $(U-U_{mf})$	(-)
n_2	Bed expansion equation factor for U_{mf}	(-)
n_3	Bed expansion equation factor for ρ_p	(-)
n_4	Bed expansion equation factor for ρ_g	(-)
n_5	Bed expansion equation factor for d_g	(-)
P	Absolute pressure	(Pa)
P^0	Reference pressure	(101325 Pa)
P_{mean}	Average pressure in the fluidized bed	(Pa)
R	Universal constant of perfect gases	$(8.314\ J.K^{-1}.mol^{-1})$
Re	Reynolds number	(-)
Re_{mf}	Reynolds number at minimum fluidization velocity	(-)
r^2	Coefficient of determination	(-)
S	Cross section of the fluidization column	(m^2)

T	Absolute temperature	(K)
T^0	Reference temperature	(273.15 K)
U	Surface velocity of the gas	($m.s^{-1}$)
U_{mf}	Minimum fluidization velocity	($m.s^{-1}$)
α	Coefficient for the bed expansion correlation	(-)
β	Coefficient for the bed expansion correlation	(-)
γ	Coefficient for the bed expansion correlation	(-)
δ	Coefficient for the bed expansion correlation	(-)
ε_{mf}	Bed porosity at minimum fluidization velocity	(-)
η_V	Viscous tortuosity	(-)
$\eta_{V,mean}$	Mean viscous tortuosity	(-)
η_K	Knudsen tortuosity	(-)
$\eta_{K,mean}$	Mean Knudsen tortuosity	(-)
μ	Viscosity	(Pa.s)
ρ_g	Density of the carrier gas	($kg.m^{-3}$)
ρ_p	Density of the particles	($kg.m^{-3}$)
σ	Molecular diameter of gas	(m)
Ψ_s	Particle sphericity	(-)
$\%_f$	Fiber mass fraction	(%)

1. Introduction

For more than 40 years, ceramic matrix composites (CMCs) have demonstrated their potential as thermostructural components in the hot sections of commercial and military jet engines [1–3]. Their thermomechanical properties would not be as high without an interfacial layer (or "interphase") between the fibers and the matrix, providing the composite a pseudo-ductile behavior [4,5]. For some specific applications of CMC where traditional woven fiber reinforcements are not be applicable, short fibers could be used. However, if CMCs are to remain damage-tolerant, the deposition process of the interphase must be compatible with such a discontinuous substrate.

CVD is typically used to deposit the interphase because of its inherent ability to coat complex shapes and porous substrates with uniform thicknesses and controlled microstructures. The process is well established for continuous substrates, such as solid parts (for the outer protective coating) or fibrous fabrics (for the CMC matrix). However, when the substrate is discontinuous, such as a bed of particles, the CVD process must be significantly redesigned to ensure a homogeneous distribution of the gas phase around all the particles, to ultimately obtain a coating of uniform composition, structure and thickness. Conventional CVD reactors typically include a hot zone where the parts to be coated or infiltrated are carefully placed so that the gases flow and react as uniformly as possible. Such a reactor design is obviously not suitable for short fibers. Conversely, it

is possible to combine a traditional CVD system with a vertical fluidization system (*i.e.*, the gas precursor inlet at the bottom and the gas effluent evacuation/treatment at the top) that simultaneously acts as a hot zone, a particle/gas mixing zone, and a deposition zone.

The fluidization process was developed at the beginning of the last century. Initially developed for ammonia production by the Haber process, fluidization later gained visibility for coal gasification and catalytic oil cracking. Coupled with CVD techniques, the process was used in the 1960s to coat the well-known TRISO fuel particles for high-temperature gas nuclear reactors [6–8]. This process succeeded in coating particulate substrates with high performance coatings at excellent yields, taking advantage of very efficient heat and mass transfer [9].

This process has been naturally chosen to coat a more original substrate here: short ceramic fibers. These particles have a high shape factor and are generally not classified in the different categories of fluidizable particles. The ability of these kind of particles to be fluidized has been mainly studied through modeling [10–16] and very few studies have described the fluidization behavior of short fibers from an experimental point of view. Furthermore, no studies have addressed the fluidization of such substrates under the specific conditions investigated here for the synthesis of interphases and protective coatings. Indeed, the specific conditions of high temperature and low pressure required are not described in the literature. A hydrodynamic study would help to clarify the specificities or similarities with other studies carried out on more classical substrates.

Preliminary experiments have shown that the geometry and the characteristic dimensions of short fibers, as well as surface interactions, lead to difficulties in maintaining a stable fluidization of a load that would consist only of short fibers. The elongation of the particles favors collisions, while their micrometric size enhances physicochemical interactions, thus preventing a proper fluidization. Due to chemical interactions or mechanical entanglements, short fibers tend to gradually agglomerate, which may eventually lead to a fixed bed. Similar observations have been reported in the case of fine cohesive spherical particles belonging to the C category according to the Geldart's classification, *e.g.* with particle diameters below 15 µm or with low density below 1000 $kg.m^{-3}$ [17]. At these scales, the surface forces are no longer negligible, which can severely affect or even prevent fluidization. Several techniques can be used to overcome these difficulties. Among them are the mechanical stirring by rotating blades inserted within the bed [18–20], the addition of acoustic vibrations towards the bed [21–24], the mechanical vibration of the whole fluidized bed support [25–28], the application of electromagnetic pulses to magnetized particles [29,30] or the addition of easily fluidizable particles to the bed [31,32]. The last solution is obviously the easiest to adapt to our equipment. It is chosen here through the

addition to the short fibers of SiC powder belonging to the A/B category according to the Geldart's classification. The interaction between these particles prevents cohesion between fibers and makes the bed more fluid, acting as a "lubricant". A few numerical studies have been carried out on mixtures of high form factor particles with near-spherical powders [13,16]. However, these models do not consider ideal hydrodynamic behavior, neglect surface forces due to physicochemical interactions between particles, and even investigate millimeter rather than micrometer particles.

We have previously investigated the fluidization behavior of a fiber/powder mixture and compared it to that of a pure powder bed [33]. The study demonstrates the possibility of fluidizing a load with a fraction of short fibers mixed with micrometric powders. It also suggests the possibility of predicting the minimum fluidization velocity using the classical Ergün's equation [34], but also using the equation of Zarekar *et al.* [35] and a modified Darcy-Klinkenberg equation. An adjustment of the experimental data has allowed us to determine, with the help of these three equations, the intrinsic properties of the fiber/powder mixture, *i.e.*:

- The hydraulic diameter ($\Psi_s d_g$), derived from the Ergün and Zarekar equations
- The Knudsen permeability (K) and diffusion coefficients (D_K), from the modified Darcy-Klinkenberg equation.

In this work, the effect of the addition of short fibers to a load initially made of powder will be examined. Several mixtures are fluidized at room temperature and at pressures ranging from 10 to 800 mbar. The monitoring of the minimum fluidization velocities is confronted with different equations adapted to the conditions used and the intrinsic properties of the mixtures are determined. The study highlights the importance of using equations adapted to hydrodynamic flow conditions. Indeed, in the case of fluidization under CVD conditions (i.e. with the use of moderate gas velocities and low pressures) the flow tends to be rarefied rather than inertial, consequently, the vast majority of U_{mf} 's prediction equations fail in their prediction. Finally, the study will propose a prediction model of U_{mf} according to simple parameters.

2. Materials and methods

The different elements of the fluidized bed reactor and the particle characteristics of the powder and short fibers have been described in detail elsewhere [33]. The hydrodynamic study was performed on SIKA® TECH silicon carbide (SiC) powders from Fiven, and Hi-Nicalon type S SiC fibers from NGS Advanced Fibers Co., Ltd. The particle size as well as the diameter and length distributions of the SiC powder and fibers are shown in Fig. 1.

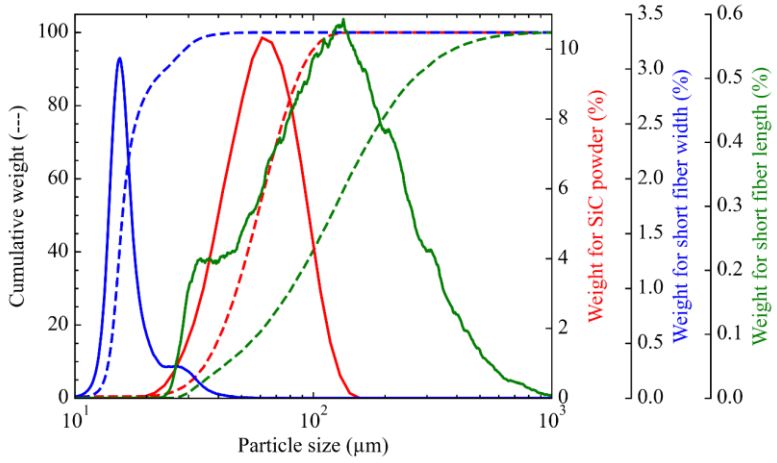

Fig. 1 : Particle sizes distributions of short fibers length, diameter and SiC powder diameter.

The mixtures are homogenized in the reactor for a few minutes to ensure optimal mixing of the particles. Fluidization tests are then performed for different short fiber/powder ratios at different pressures. For each pressure and each fiber/powder ratio, the plot of the bed pressure drop as a function of the decreasing carrier gas velocity (*e.g.* nitrogen) provides the minimum fluidization velocity (U_{mf}). Furthermore, measurements of the bed height at different velocities are used to determine the normalized expansion and the porosity of the bed at the minimum fluidization velocity. The bed height is measured using a graduated ruler placed next to the quartz fluidization column. The height is determined as the average of the maximum and minimum heights of the bed along the column walls during the fluidization process.

2.1. Hydrodynamic laws

Several authors have been interested in predicting the minimum fluidization velocity using reference equations, semi-empirical correlations or numerical modeling. It is difficult to compare and evaluate the relevance of all of these studies since each author uses specific fluidization operating conditions. All correlations are specific to particular experimental conditions, either by using different pressures, temperatures, particles with variable physical and geometrical properties, etc... Nevertheless, a significant number of studies are based on the semi-empirical correlation derived from the Ergün equation. This correlation proposes to relate the dimensionless Reynolds number: $Re_{mf} = (U_{mf}\rho_g d_g)/\mu$ and the Archimedes number: $Ar = (g(\rho_p-\rho_g)\rho_g d_g^3)/\mu^2$ numbers by the following Equation (1).

$$Re_{mf} = \sqrt{A^2 + BAr} - A \qquad \textit{Equation (1)}$$

Equation (1) is derived from the numerical solution of the Archimedes number equation as a function of Reynolds number, see Equation (2).

$$Ar = K_1 Re_{mf}^2 + K_2 Re_{mf}$$ ***Equation (2)***

Where K_1 and K_2 are the inertial and laminar flow coefficients, respectively, and A and B are the coefficients resulting from the numerical solution of Equation (2), *i.e.* $A = K_2/(2K_1)$ and $B = 1/K_1$. Many authors propose values for these last coefficients, some of them are listed in Table 1.

Table 1 : Values of the A and B coefficients for the calculation of the minimum fluidization.

Authors	Parameters	
	A	*B*
Babu *et al.* [39]	25.25	0.0651
Bourgeois and Grernier [37]	25.46	0.0384
Chitester *et al.* [42]	28.70	0.0494
Richardson and Jerónimo [40]	25.70	0.0365
Saxena and Vogel [38]	25.28	0.0571
Tannous *et al.* [43]	25.83	0.0430
Thonglimp *et al.* [41]	31.60	0.0452
Wen and Yu [36]	33.70	0.0408

Under subatmospheric pressure fluidization conditions, and especially at low pressures (*e.g.* < 50 mbar), other studies [44,35,45] emphasize the relationship between the coefficient K_2 in Equation (2) and the Knudsen number: $Kn = (K_B T)/(\sqrt{2}\pi\sigma^2 P d_p)$. For example, Zarekar *et al.* [35] propose an inverted second-order polynomial equation of the form $K_2 = (7.10.10^{-4} + 6.25.10^{-3}Kn + 3.52.10^{-3}Kn^2)^{-1}$. Weesasiri *et al.* [45] propose a linear dependence of the form: $K_2 = 2.52.10^3 - 7.53.10^4 Kn$. Finally, Llop *et al.* [44] distinguish two cases depending on the sphericity of the particles. In the case of near-spherical particles ($\Psi_s > 0.8$): $K_2 = (6.06.10^{-4} - 1.98.10^{-2}Kn)^{-1}$ and in the case of non-spherical particles ($0.4 > \Psi_s > 0.8$): $K_2 = (7.41.10^{-4} - 1.51.10^{-2}Kn)^{-1}$. These considerations best approximate the peculiar behavior of the minimum fluidization velocity at low pressure, by the Knudsen number proportional to P^{-1}.

The mathematical developments of the Ergün and modified Darcy-Klinkenberg equations have been described in detail elsewhere [33] and the results are respectively summarized below, see Equations (3) and (5). The equation of Zarekar *et al.* [35] has also been considered in its most complete form by introducing the squared Knudsen term, *i.e.* $4.96Kn^2$, representing the rarefied flow, which cannot be neglected at low pressure, see Equation (4).

The Ergün equation is described below:

$$U_{mf} = \sqrt{\left(\frac{150\mu(1-\varepsilon_{mf})}{3.5\rho_g(\Psi_s d_g)}\right)^2 + \frac{\varepsilon_{mf}^3(\rho_p - \rho_g)g(\Psi_s d_g)}{1.75\rho_g}} - \frac{150\mu(1-\varepsilon_{mf})}{3.5\rho_g(\Psi_s d_g)}$$ ***Equation (3)***

As well as the Zarekar's equation:

$$U_{mf} = \sqrt{\left(\frac{25.7\mu}{\rho_g(\Psi_s d_g)(1 + 8.8Kn + 4.96Kn^2)}\right)^2 + 0.0365\frac{(\rho_p - \rho_g)g(\Psi_s d_g)}{\rho_g}} - \frac{25.7\mu}{\rho_g(\Psi_s d_g)(1 + 8.8Kn + 4.96Kn^2)} \quad \textit{Equation (4)}$$

And the Darcy-Klinkenberg equation:

$$U_{mf} = (\rho_p - \rho_g)(1 - \varepsilon_{mf})g\left[\frac{K}{\mu} + \frac{D_K}{P_{mean}}\right] \quad \textit{Equation (5)}$$

2.2. Methodology

Our previous study showed a limited effect of the temperature on U_{mf} compared to that of the pressure (especially at low pressures). Therefore, in the present study, the minimum fluidization rate was evaluated only as a function of the pressure (from 10 to 800 mbar) at room temperature. These experiments allow the direct visualization of the fluidized bed through the quartz column. Moreover, the surface interactions between the particles are limited at room temperature (as opposed to high temperatures where surface reactions are activated), which allows to stabilize the fluidization behavior of the bed during the experiments. Variables such as the density (ρ_g) or carrier gas viscosity (μ) are calculated under the considered temperature and pressure conditions. The porosity at minimum fluidization is derived from the bed expansion measurements using Equation (6).

$$\varepsilon_{mf} = 1 - \frac{m}{\rho_p S H_{mf}} \quad \textit{Equation (6)}$$

Where m is the mass of the fluidized bed, S is the cross-sectional area of the fluidization column, H_{mf} is the absolute height of the fluidized bed at minimum fluidization conditions, and ρ_p is the particle density. Therefore, for each fiber fraction in the mixture and for each pressure, ε_{mf} can be calculated. This value at minimum fluidization velocity varies only slightly with pressure. An average value of ε_{mf} can then be deduced for each short fiber/powder ratio, regardless of the pressure considered.

The Levenberg-Marquardt algorithm, developed by Levenberg [46] in 1944 and published by Marquardt [47] in 1963, provides a numerical solution to the problem of minimizing nonlinear functions dependent on one or more variables. The algorithm, based on the Gauss-Newton methods and the gradient algorithm, minimizes the sum of squares of the deviations between the experimental and the fitted data (least squares minimization). This method is used here to fit the intrinsic parameters of the different particle loads, via the equations proposed above, see Equations (3), (4) and (5). The algorithm also provides the standard deviation of each parameter.

The minimum fluidization velocities (U_{mf}) are determined from the pressure drop curves at decreasing flow rates and using an algorithm for determining the pressure drop slope at low flow rates and the plateau at the highest flow rates. This algorithm performs two linear regressions, giving access to U_{mf} and the error associated with the fit. From the experimental values of the minimum fluidization velocity as a function of pressure (P), a regression of the Ergün and Zarekar equations directly yields the product $\Psi_s d_g$. However, it is important to note that the Ergün equation does not take into account the experimental data at low pressure (*i.e.* where the rarefied regime is no longer negligible). In fact, the Ergün equation considers laminar to inertial flow and therefore does not consider the modifications of U_{mf} in the case of a flow that tends to become rarefied (which is actually the case at P < 100 mbar, where the contribution of the rarefied flow is at least 20%). Conversely, the Zarekar and modified Darcy-Klinkenberg equations integrate the rarefied flow at low pressures. Therefore, the low-pressure experimental points should be carefully considered for variable adjustment.

While both Ergün's and Zarekar's equations are able to account for the evolution of the hydraulic diameter ($\Psi_s d_g$) as a function of the fiber fraction in the mixtures, the Darcy-Klinkenberg equation only provides an estimation of the permeability coefficient $K = (\varepsilon_{mf}^3 d_g^2)/(32\eta_V(1-\varepsilon_{mf})^2)$ and the Knudsen diffusion coefficient $D_K = (\varepsilon_{mf}^2 c d_g)/(3\eta_K (1-\varepsilon_{mf}))$, as a function of the fiber fraction. These coefficients involve two different corrective terms, which are equivalent to the sphericity (Ψ_s) of the particles in the Ergün and Zarekar equations: the viscous and Knudsen tortuosities, respectively η_V and η_K. At this stage, it is difficult to introduce a sphericity of the fibers or the mixtures, by analogy to that of the powder, in order to introduce it in the fitted hydraulic diameter values. Sphericity is a parameter that is relevant in the case of powder alone, but the elongated and cylindrical geometry of the short fibers may require the introduction of another more appropriate shape factor to correct the grain diameter (d_g).

Fluidized bed expansion can be followed as a function of several parameters including the gas velocity excess ($U-U_{mf}$), the minimum fluidization velocity (U_{mf}), the particle density (ρ_p), the gas density (ρ_g), or even the grain diameter (d_g). Several authors have proposed their own empirical correlation, using some or all of the latter parameters [42,48–50]. The general form and the coefficients proposed by some authors have been described elsewhere [33]. The general equation can be recalled as follows in Equation (7).

$$H^* = \frac{H}{H_{mf}} = 1 + \alpha(U - U_{mf})^{n_1} U_{mf}^{n_2} \rho_p^{n_3} \rho_g^{n_4} d_g^{n_5} \qquad \textit{Equation (7)}$$

In our previous study [33], the coefficients $n_1 = 1$ and $n_4 = 0.2108 \pm 0.0313$ have been proposed for two different types of load, the first one consisting only of powder and the second one of a certain fiber fraction in the mixture. In the present case, the variation of the short fiber fraction in the mixture allows to vary the diameter of the load while keeping the other parameters fixed, in order to deduce the exponent n_5.

3. Results

3.1. Velocities and porosities at minimum fluidization

The hydrodynamic study investigates the effect of adding particles with a high shape factor (short fibers) to a powder with a shape factor close to 1. Six different mixtures have been submitted to fluidization tests with increasing fiber mass ratios from 0 to 15%, corresponding to bulk volume fractions of 0 to 30.1% or tapped volume fractions of 0 to 26.1%, respectively, see Table 2. Each mixture is subjected to the gas flow at several pressures (ranging from 10 to 800 mbar) and the pressure drop between the bottom and the top of the bed is plotted against the decreasing gas velocity.

Table 2 : Mass, bulk and tapped percentages of fibers in fiber/powder mixtures.

Fiber mass fractions	0%	2.5%	5.0%	7.5%	10.0%	15.0%
Fiber bulk volume fractions	0%	5.9%	11.4%	16.5%	21.3%	30.1%
Fiber tapped volume fractions	0%	4.9%	9.5%	13.9%	18.2%	26.1%

The variation of the pressure drop with the decreasing gas velocity allows the determination of the minimum fluidization velocity U_{mf}, for all pressures and fiber fractions considered. These minimum fluidization velocities are plotted against pressure in Fig. 2. The contribution of the rarefied flow increases as the fluidization pressure decreases. In fact, below 100 mbar, the minimum fluidization velocity increases rapidly (up to almost 250%). For pressures above 100 mbar, U_{mf} remains stable. The addition of fibers to the mixture generally results in a decrease of U_{mf}, *e.g.* in the range of 100-800 mbar: $U_{mf} = 29$ cm.min^{-1} without fibers, versus 14 cm.min^{-1} with 15 mass % of fibers, *i.e.*, a reduction of U_{mf} of approximately 50%.

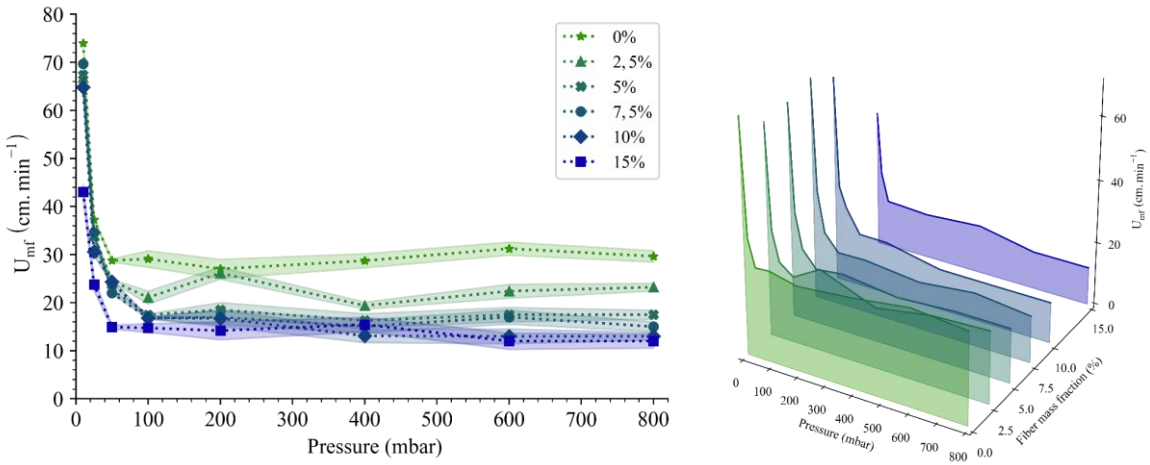

Fig. 2 : Minimum fluidization velocity (U_{mf}) as a function of pressure for various fiber/powder mixtures (error bars appear as colored beams delimited by the low and high values for each experimental point).

The measurement of the normalized bed height ($H^* = H/H_{mf}$) can be used to determine its porosity, especially at the minimum fluidization velocity (ε_{mf}, Equation (6)). Fig. 3 shows the evolution of ε_{mf} as a function of the short fiber mass fraction. The addition of fibers gradually decreases the bed porosity at the minimum fluidization velocity. The porosity ε_{mf} indeed decreases from 0.633 without fibers to 0.590 with 15 mass % fibers, *i.e.* a reduction of about -7%.

This tendency may be surprising since short fibers are more elongated than powder particles. The diameter of the fibers being lower than that of the powder particles, short fibers added at low percentages will fill the space between the particles (especially the shortest fibers between the largest particles), resulting in a decrease in porosity. On the other hand, since a pure short fiber bed has a higher porosity than a pure powder bed, it would not be surprising to find that the porosity of a high-fiber fraction mixture tends to increase with the amount of added fibers. Unfortunately, these high-fraction mixtures could not be studied because of their unsuitability for fluidization. In fact, a channeling phenomenon gradually occurred, the bed becoming static and thus the pressure drop curves could not be exploited.

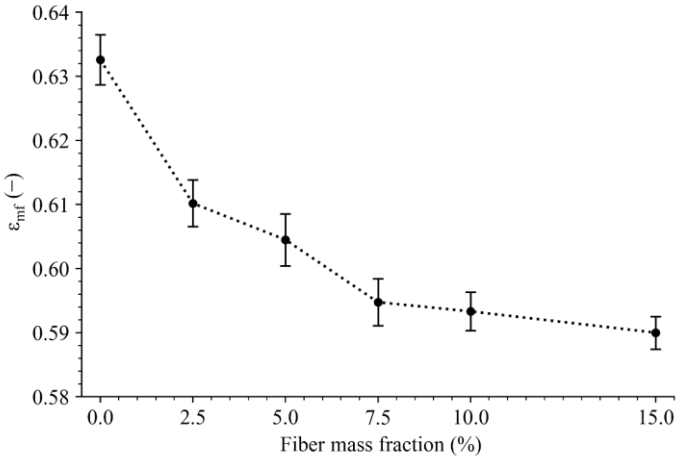

Fig. 3 : Evolution of the average porosity at minimum fluidization (ε_{mf}) as a function of the fiber fraction in the mixture.

3.2. Ergün and Zarekar equations

The variable $\Psi_s d_g$ represents the hydraulic diameter and is similar to the sphere diameter of the equivalent surface-to-volume ratio: d_{sv} (or Sauter diameter). $\Psi_s d_g$ is also the main fitting parameter for the Ergün and Zarekar hydrodynamic equations, see Equations (3) and (4). This quantity is fitted and plotted for each $U_{mf}(P)$ curve and each fiber/powder ratio, assuming an Ergün or Zarekar type relationship, see Fig. 4. The fit, based on the Ergün equation, gives lower $\Psi_s d_g$ values (34 to 29 µm) than for the Zarekar equation (61 to 43 µm). In both cases, the hydraulic diameter tends to decrease as the mass fraction of fibers increases. This trend indicates that in terms of fluidization, the equivalent size of the particle mixture felt by the gas stream decreases as the fiber mass fraction increases, which is consistent with the decrease of the minimum fluidization velocity observed simultaneously.

The difference between the results of the Zarekar and Ergün equations, see Fig. 4, lies in the basic considerations for applying these two equations. For instance, the Ergün's equation includes empirical corrective factors found in Equation (3), which are of the form: 150/3.5 for the Darcy laminar flow part and 1/1.75 for the Forchheimer inertial flow part, while Zarekar uses the Richardson's correlated coefficients [40] 25.7 and 0.0365, in addition to the correction for rarefied flow via the Knudsen dimensionless number, of the following expression: $1 + 8.8Kn + 4.96Kn^2$. These different considerations inevitably imply different results for the hydraulic diameter.

The sphericity value (Ψ_s) acts as a corrective coefficient for the physical particle diameter (d_g). However, it is impossible to calculate or even estimate by any means the sphericity value of a powder and short fiber mixture. Moreover, there is no evidence that sphericity as defined by Wadell [51], remains the relevant corrective factor to describe the behavior of the mixture after the addition of fibers. Assuming that sphericity is indeed the

corrective factor to be considered, assigning a specific value for a mixture of particles of very different geometries (in this case a powder and fibers), simply from their respective mass fractions, may seem inappropriate given the complexity of the problem. It was therefore decided to keep the whole $\Psi_s d_g$ product as the main variable of interest for the hydrodynamic calculations.

The hydraulic diameter can be related to the fiber mass fraction to deduce the corresponding minimum fluidization velocity. For this purpose, it was decided to use the data derived from the fitting of the Zarekar equation. The chosen equation is of the form: $\Psi_s d_g = a(\%_f + b)^n$, where a and b are positive coefficients and n a negative coefficient with an absolute value less than 1. The hydraulic diameter $\Psi_s d_g$ is approximated by the Sauter diameter d_{sv}. In this case, without fibers, the hydraulic diameter is equal to the Sauter's diameter of the powder: $\Psi_s d_g(0\%_f) = d_{sv}^{\ p}$, while with the fibers only it becomes: $\Psi_s d_g(100\%_f) = d_{sv}^{\ f}$. Under these conditions, it comes:

$$\begin{cases} \Psi_s d_g(0\%_f) = a(\%_f + b)^n = d_{sv}^p \\ \Psi_s d_g(100\%_f) = a(\%_f + b)^n = d_{sv}^f \end{cases} \qquad \textit{Equation (8)}$$

With the respective fiber mass fractions:

$$\begin{cases} ab^n = d_{sv}^p \\ a(1+b)^n = d_{sv}^f \end{cases} \qquad \textit{Equation (9)}$$

That is to say:

$$\begin{cases} a = d_{sv}^p \left[\left({d_{sv}^f}/{d_{sv}^p} \right)^{n^{-1}} - 1 \right]^n \\ b = \left[\left({d_{sv}^f}/{d_{sv}^p} \right)^{n^{-1}} - 1 \right]^{-1} \end{cases} \qquad \textit{Equation (10)}$$

The Sauter diameter of the fibers and the powder are obtained from optical microscopy images. Each image is processed individually by a powder or fiber edge detection algorithm. The entities partially masked or cut-off by the edges of the image frame are removed. Analysis of the closed contours provides the projected area of each particle and allows to calculate the ratio between the measured projected area and the equivalent spherical volume. A series of images is used to obtain an average of the measurements.

The fitting parameter for the variable n yields a satisfactory correlation ($r^2 = 0.9860$), see Fig. 4, with $d_{sv}^{f} = 25.0 \pm 0.8$ µm, $d_{sv}^{p} = 61.1 \pm 1.0$ µm and $n = -0.35 \pm 0.01$, which allows the prediction of the hydraulic diameter for any ratio of fibers in the fiber/powder mixture.

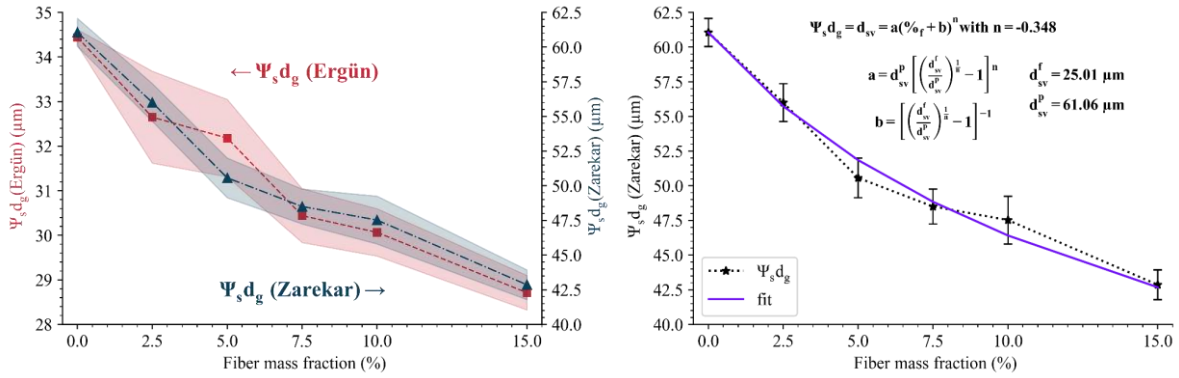

Fig. 4 : Evolution of hydraulic diameter ($\Psi_s d_g$) (left) and Zarekar hydraulic diameter fit as a function of fiber mass fraction in the mixture (right).

3.3. Darcy-Klinkenberg equation

The variable fitting parameter of the experimental data, taking into account the Darcy-Klinkenberg equation, allows the evaluation of the permeability coefficients K and D_K at any fiber/powder ratio, see Fig. 5. The permeability K decreases by a factor of about 2 as the fiber mass fraction increases from 0 to 15%. In contrast, the Knudsen coefficient D_K does not show a monotonic behavior as a function of the fiber mass fraction. This unexpected behavior is difficult to explain, as D_K depends simultaneously on Knudsen tortuosity, molecular velocity and pore diameter. The results also show that it might be due to experimental errors. From these coefficients and the porosities at the fluidization minimum, it is possible to obtain the quantities: d_g^2/η_V with K and d_g/η_K with D_K, see Fig. 6. Again, these quantities do not show a clear monotonic variation with the fiber mass fraction.

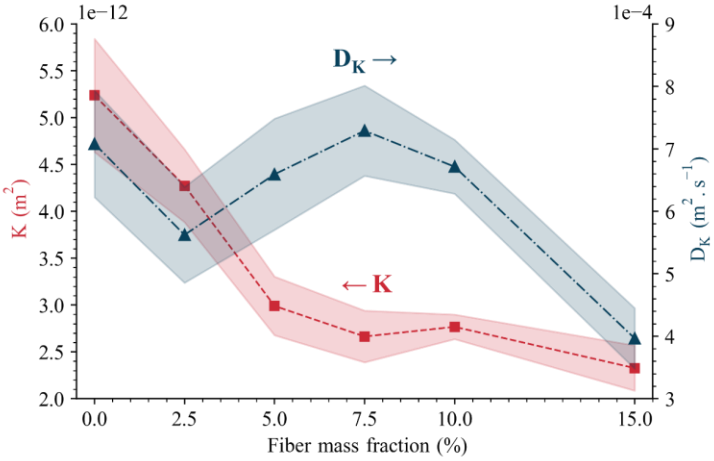

Fig. 5 : Evolution of the permeability coefficient (K) and Knudsen coefficient (D_K) as a function of the fiber mass fraction in the mixture.

Like the sphericity (Ψ_s) in the Ergün and Zarekar equations, the viscous and Knudsen tortuosities (η_V and η_K) act as corrective factors towards the grain diameter (d_g) in the Darcy-Klinkenberg equation. Since it is not possible to deduce the tortuosities experimentally without a specific study of the porous medium, it was decided to use the empirical correlation found previously for $\Psi_s d_g$ instead of the grain diameter (d_g) in the Darcy-Klinkenberg equation. In this case, the tortuosities lose their corrective characters and become constant with the variation of the fiber mass fraction. Under this condition, η_V and η_K are plotted as a function of the fiber mass fraction, see Fig. 6. The calculated tortuosities appear relatively constant as a function of fiber mass fraction. Therefore, the mean values $\eta_{V,mean}$ and $\eta_{K,mean}$ can be calculated and used in the Darcy-Klinkenberg equation, where the grain diameter (d_g) is replaced by the hydraulic diameter ($\Psi_s d_g$) previously fitted.

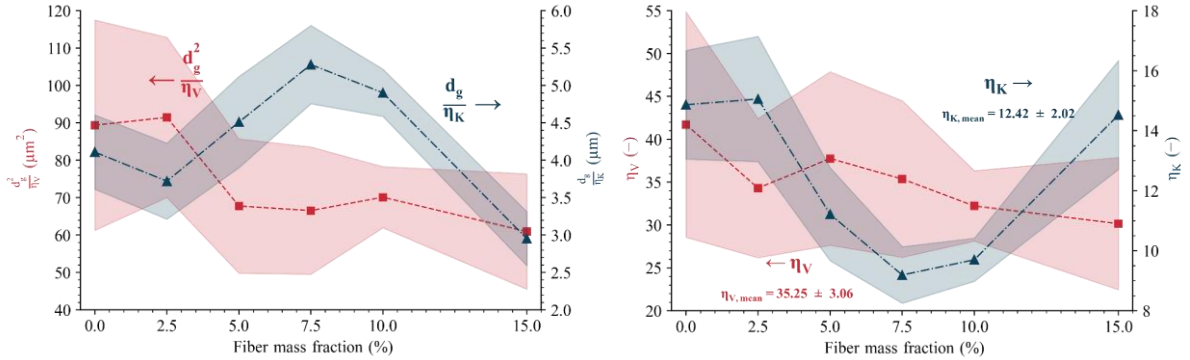

Fig. 6 : Evolution of the proportions d_g^2/η_V and d_g/η_K (left) and the tortuosities η_V and η_K (right) as a function of the mass fraction of fiber in the mixture.

The calculated tortuosities are also plotted against each other, see Fig. 7. Charles *et al.* [52] showed that viscous and Knudsen tortuosities are correlated with each other in fibrous media, with the same correlation regardless of the orientation of the fibers and the gas path. Charles *et al.* suggest a correlation between viscosity and Knudsen

tortuosities of the form: $\eta_V = 2.3\eta_K^{1.05}$. Considering the errors of η_V and η_K, the proposed correlation is in good agreement with the experimental data. The mean tortuosities, *i.e.* $\eta_{V,mean}$ and $\eta_{K,mean}$, deviate from the prediction by only 8%.

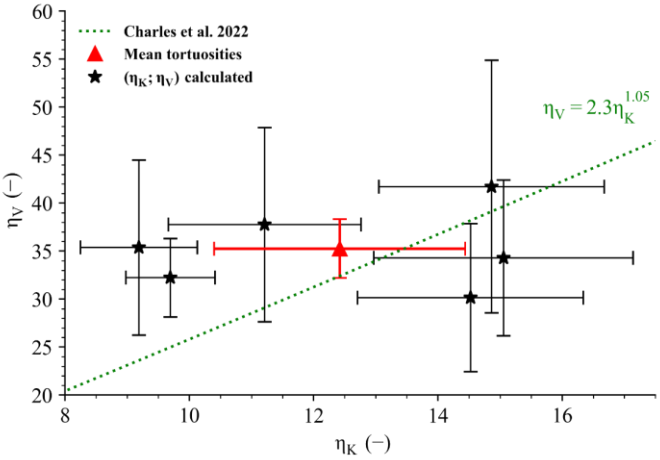

Fig. 7 : Viscous against Knudsen tortuosities plotted with Charles et al. correlation.

The resulting Darcy-Klinkenberg equation can be rewritten in the following form:

$$U_{mf} = (\rho_p - \rho_g)(1-\varepsilon_{mf})g\left[\frac{1}{\mu}\frac{\varepsilon_{mf}^3(\Psi_s d_g)^2}{32\eta_{V,mean}(1-\varepsilon_{mf})^2} + \frac{1}{P_{mean}}\frac{\varepsilon_{mf}^2 c(\Psi_s d_g)}{3\eta_{K,mean}(1-\varepsilon_{mf})}\right] \qquad \textit{Equation (11)}$$

3.4. Bed expansion

The expansions are first fitted for each pressure and each fiber/powder ratio, with the following equation: $1 + \beta(U\text{-}U_{mf})$. Then, the coefficients β are plotted as a function of gas density for each pressure considered, for all fiber mass fractions. The curves obtained are then fitted again with a function of the type: $\beta = \gamma\rho_g^{n4}$. This second fitting parameter allows to obtain the coefficients γ and n_4 for each fiber mass fraction, see Fig. 8. There is a very minor increase of n_4 as a function of the fiber mass fraction, probably indicating the effect of another parameter, not considered here. In the following, an average n_4 coefficient equal to 0.096 ± 0.090 will be considered. On the other hand, the coefficient γ contains information related to the other parameters mentioned before such as ρ_p, which remains constant here. For example, it is possible to determine the contribution of the equivalent hydraulic diameter to the bed expansion by a new variable fitting. The coefficient γ is thus plotted as a function of $\Psi_s d_g$, and a variable fitting is performed with a function of the type: $\gamma = \delta(\Psi_s d_g)^{n5}$, see Fig. 8. The fitting yields results correlated with the experimental data (r^2 = 0.9794) with an exponent n_5 = -3.309 ± 0.263 and a factor $\delta = 1.75.10^{-14} \pm 4.58.10^{-14}$.

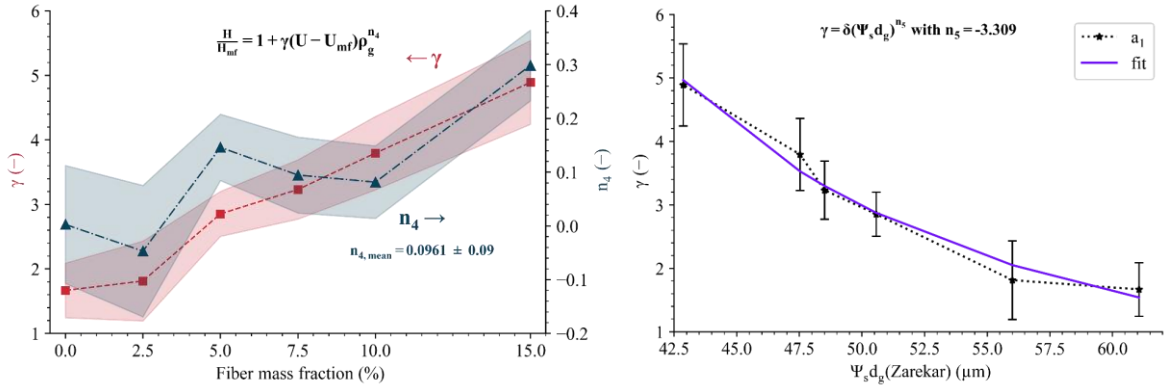

335

336 ***Fig. 8 : Evolution of γ and n_4 coefficients as a function of fiber mass fraction in the mixture (left) and fit of γ as a function of $\Psi_s d_g$ from***

337 ***Zarekar (right).***

$$H^* = \frac{H}{H_{mf}} = 1 + 1.75.10^{-14}(U - U_{mf})^1 \rho_g^{0.096} \left(\Psi_s d_g\right)^{-3.309} \qquad \textit{Equation (12)}$$

338 The expansion of the bed can be summarized as follows:

339 Fig. 9 shows the fluidized bed expansions determined at different pressures and for the different fiber mass
340 fractions considered here. The correlations proposed by Chitester *et al.* [42], Feng *et al.* [48], Lewis *et al.* [49]
341 and Rashid *et al.* [50] are also plotted by approximating the grain diameter (d_g) to the equivalent hydraulic
342 diameter ($\Psi_s d_g$) found via the Zarekar equation. The fluidized bed expansion determined experimentally
343 increases with the fiber mass fraction and pressure, indicating that the coefficient n_4 tends to be positive while
344 the coefficient n_5 is negative (when the fiber fraction increases, the equivalent hydraulic diameter decreases).

345 Fig. 10 shows the relative errors made between the numerical calculations deduced from the different
346 correlations and the experimentally measured fluidized bed expansions. The correlations proposed by Feng *et al.*
347 and Rashid *et al.* deviate strongly from the measured fluidized bed expansions. For all pressures and all fiber
348 mass fractions, the correlation of Chitester *et al.* underestimates the expansion by about 10%. The correlation of
349 Lewis *et al.* and the one proposed here, see Equation (13), are in much better agreement with the experimental
350 data for all pressures and all fiber mass fractions.

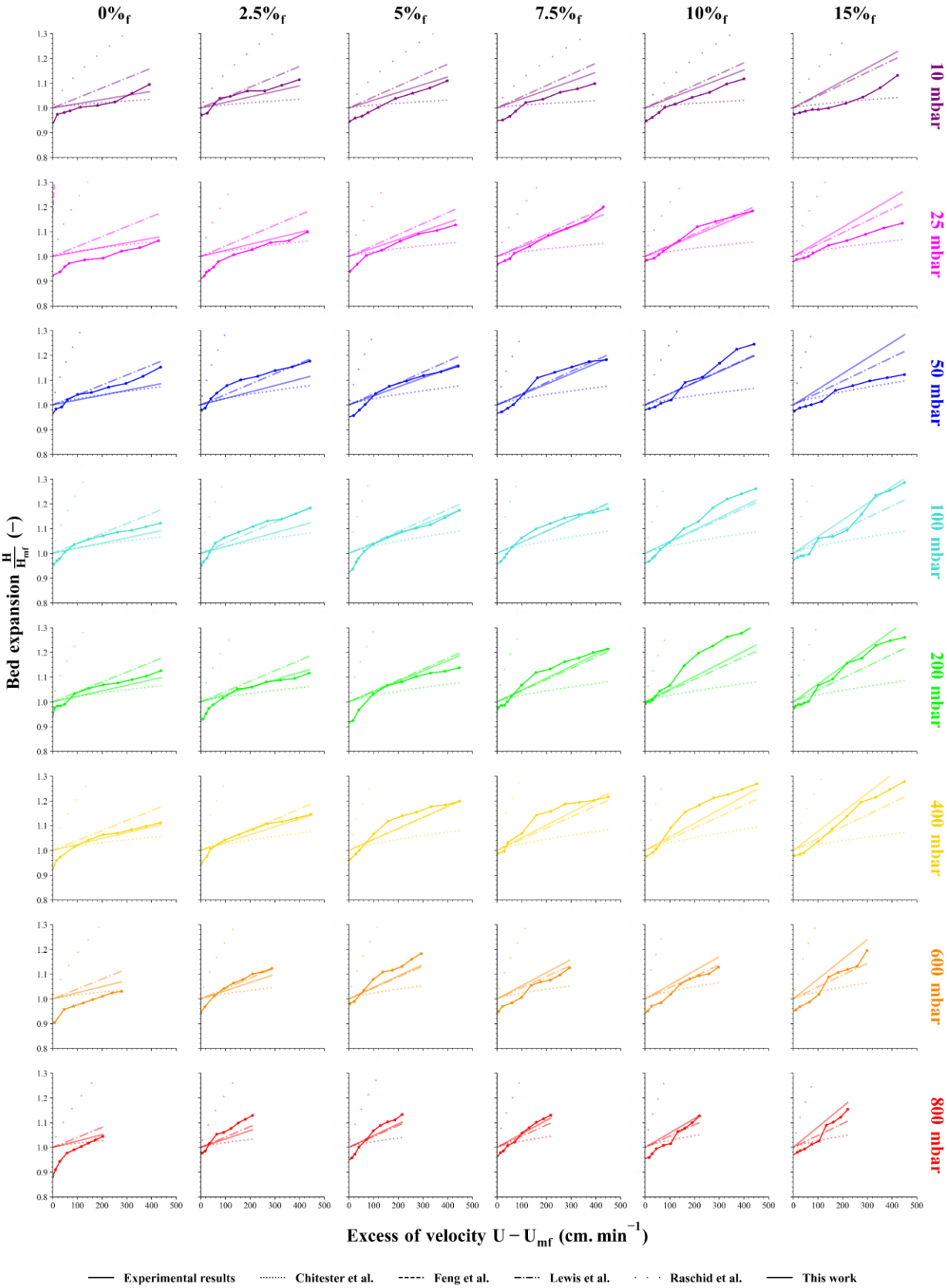

351

352 ***Fig. 9 : Expansions H/H_{mf} as a function of gas velocity.***

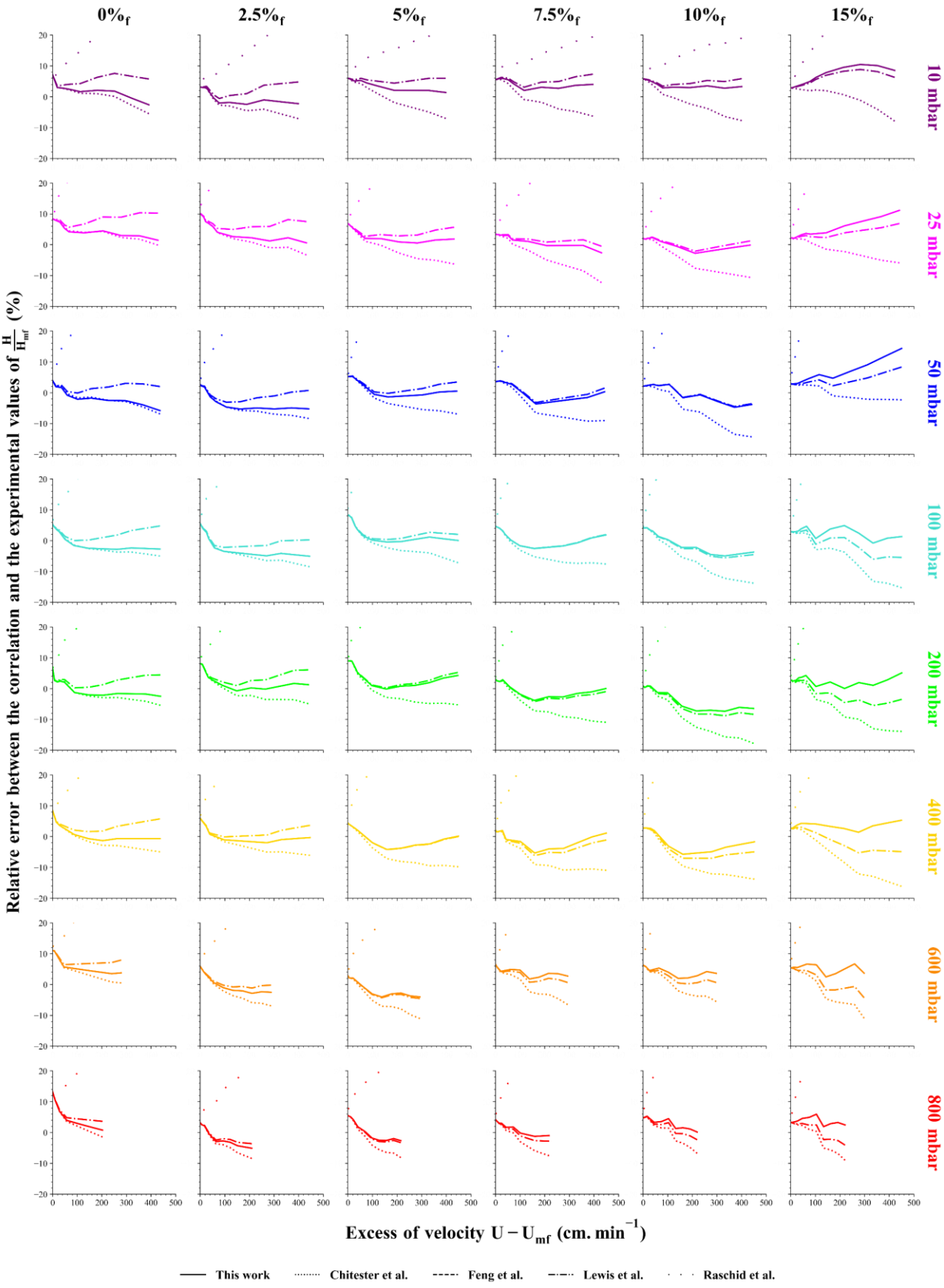

353

354 ***Fig. 10 : Relative error of the expansions H/H_{mf} as a function of gas velocity for Chitester, Feng, Lewis, Raschid and this work.***

355

4. Discussion

4.1. Prediction of the minimum fluidization velocity with Zarekar and Darcy-Klinkenberg

From the previously found fitting parameter of $\Psi_s d_g$ as a function of the fiber mass fraction and the experimental determination of the porosity at the minimum fluidization (ε_{mf}), it is possible to determine the minimum fluidization velocity for each mixture considered using the Ergün and Zarekar equations. Nevertheless, the Ergün's equation will not be considered here because of the assumptions about the flow that it requires. Indeed, Ergün bases his semi-empirical equation on Darcy and Forchheimer flows, *i.e.* laminar to inertial flows. In reality, under the usual conditions of the fluidized bed and the types of load experienced in this study, the flows involved are rather laminar-rarefied than laminar-inertial.

The experimental data are confronted with the data calculated by the Zarekar equation, using the experimentally determined porosities at the fluidization minimum and the hydraulic diameter obtained previously by fitting, see Fig. 11. Similarly, with the Darcy-Klinkenberg equation and using ε_{mf}, $\Psi_s d_g$, and the mean tortuosities $\eta_{V,mean}$ and $\eta_{K,mean}$, it is possible to calculate the minimum fluidization velocities as a function of the pressure and the fiber mass fraction, see Fig. 11. In the case of the Zarekar equation, the calculated minimum fluidization velocities agree with the experimental data, except for the lowest pressures (10 and 25 mbar). In the latter case, the calculated minimum fluidization velocities underestimate the experimental velocities by about 40%, with a maximum error of about 60% at 10 mbar, for a fiber mass fraction of 10%. For the Darcy-Klinkenberg equation, the calculated and experimental data match for the entire pressure range and for all fiber fractions. Below 50 mbar, the Darcy-Klinkenberg equation clearly gives a better prediction than the Zarekar equation.

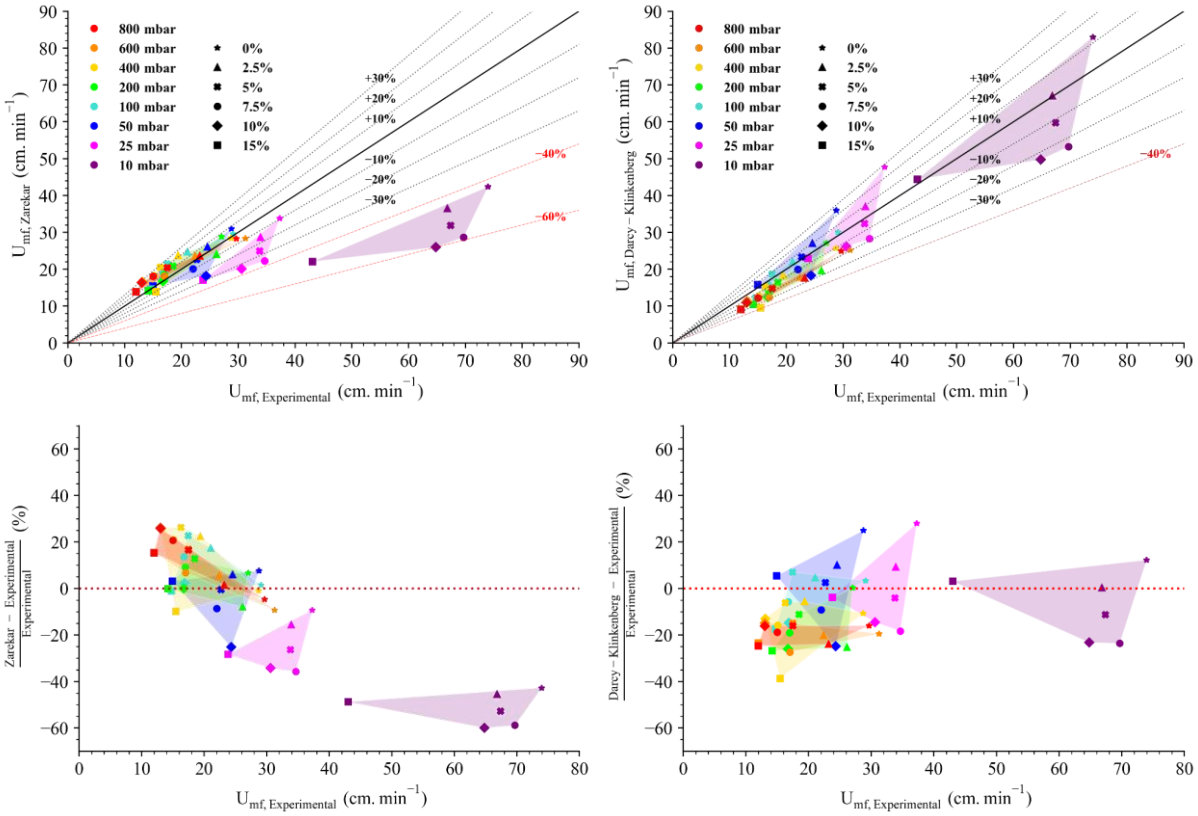

375

376

377 ***Fig. 11 : Comparisons of experimental and calculated minimum fluidization velocities (top) with Zarekar (left) and Darcy-Klinkenberg***

378 ***(right). Relative errors made by the calculation compared to the experimental values (bottom) with Zarekar (left) and Darcy-Klinkenberg***

379 ***(right).***

380 The average errors as well as the extreme errors (minimum and maximum) made between calculated and

381 experimental values are plotted as a function of the working pressure for both Zarekar and Darcy-Klinkenberg

382 equations, see Fig. 12. Again, the Darcy-Klinkenberg equation is more efficient in describing U_{mf} at low

383 pressures (< 100 mbar), although the two equations are very similar in terms of the relative error at pressures

384 greater or equal to 100 mbar. The only notable difference is the overestimation or underestimation of the value of

385 the minimum fluidization velocity. In fact, while the Zarekar equation seems to slightly overestimate U_{mf} by

386 10%, the Darcy-Klinkenberg equation underestimates U_{mf} by about 15%. The Zarekar's equation is then quite

387 satisfactory for pressures greater than or equal to 100 mbar and has the advantage of not requiring any

388 assumption about the tortuosity values of the porous medium.

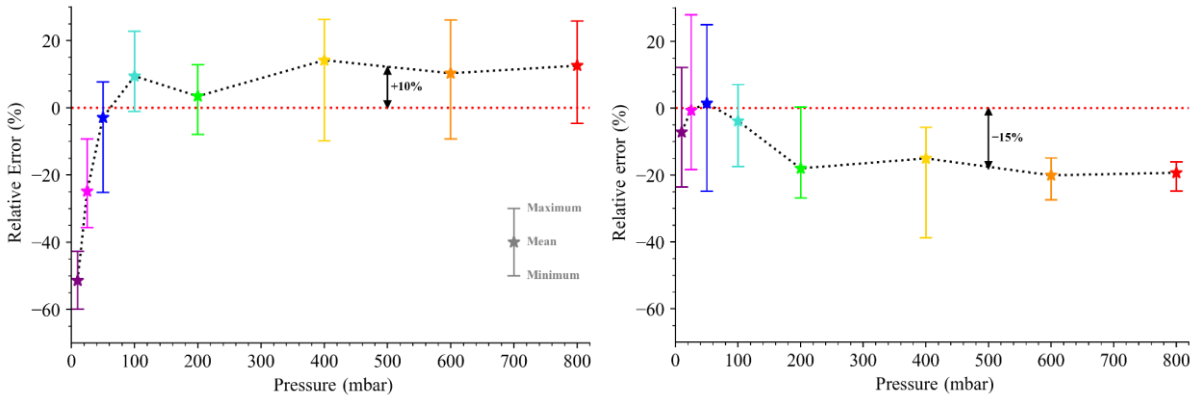

Fig. 12 : Average errors with minimum and maximum errors of the calculations with Zarekar (left) and Darcy-Klinkenberg (right) for each pressure.

While the Ergün equation is inadequate for predicting the minimum fluidization velocity at reduced pressures and rarefied flows, the Zarekar and Darcy-Klinkenberg equations better describe the variations of U_{mf}, see Fig. 13. At pressures above 100 mbar, using the Zarekar equation, see Equation (4), instead of the modified Darcy-Klinkenberg equation, see Equation (11), results in an average error of 33%. At 10 mbar, for any fiber fraction, the error increases and reaches an average of -61%, *i.e.* a severe underestimation of the minimum fluidization velocity.

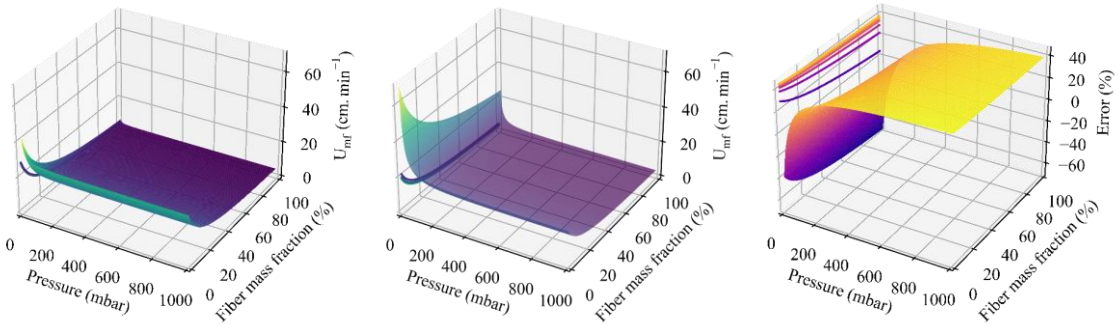

Fig. 13 : Predictions of U_{mf} as a function of pressure and fiber mass fraction with Zarekar (left); Darcy-Klinkenberg (middle) and the error made by considering the Zarekar equation rather than the Darcy-Klinkenberg one with ε_{mf} = 0.6 (right).

From the values of U_{mf}, the temperature/pressure conditions, and the $\Psi_s d_g$ values, it is possible to calculate the Reynolds (Re) and Archimedes (Ar) numbers. These two dimensionless numbers are plotted against each other in Fig. 14. In addition to these data, the semi-empirical correlations listed in Table 1 are also plotted. The hydrodynamic considerations of the semi-empirical equations are obviously not valid below 50 mbar. The points derived from the minimum fluidization values measured at low pressures (≤50 mbar) deviate from the behavior

expected by the semi-empirical correlations proposed by the different authors. Beyond this deviation, it is the form of Equation (1) itself that no longer allows to describe the particular behavior observed at low pressure.

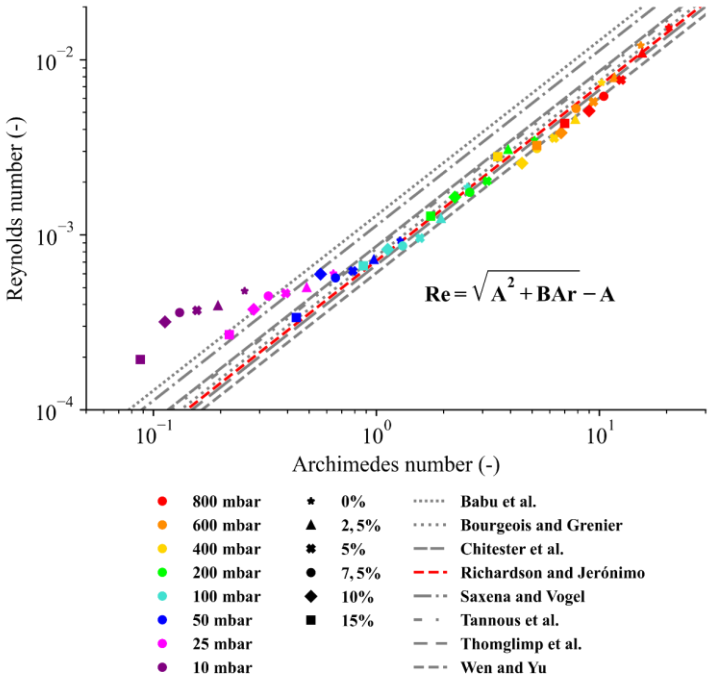

Fig. 14 : Reynolds number: $Re_{mf} = (U_{mf}\rho_g\Psi_s d_g)/\mu$ as a function of the Archimedean number: $Ar = (g(\rho_p-\rho_g)\rho_g(\Psi_s d_g)^3)/\mu^2$.

4.2. Prediction of the minimum fluidization velocity with semi-empirical correlation

Previous studies [35,44,45] have highlighted the dependence of the K_2 coefficient on the Knudsen number. Here again, it is possible to observe a dependence and establish a correlation between these two values, see Fig. 15. A nonlinear regression of an inverted second-degree polynomial was then proposed, in the form: $K_2 = (c_2Kn^2 + c_1Kn + c_0)^{-1}$. Other forms of fitting parameters have been tested, but they were either insufficient to describe the low-pressure points, or too complex (overfitting) and therefore physically inconsistent (*e.g.* non-monotonic). The results of this regression are plotted in Fig. 15 as a black dashed line, along with the correlations proposed by Weesasiri, Zarekar and Llop.

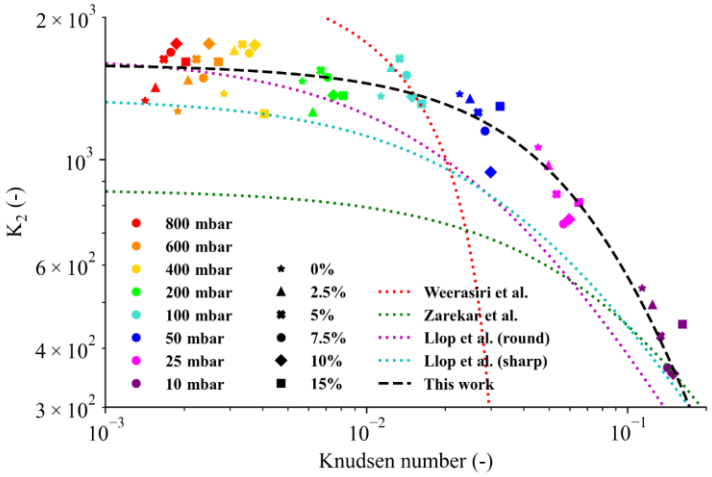

418

419 ***Fig. 15 : Variable K_2 as a function of the Knudsen number: $Kn = (K_B T)/(\sqrt{2}\pi\sigma^2 P d_p)$.***

420 The graph clearly shows that the correlations proposed by other authors are not adequate to describe the
421 experimental data found in this study. Conversely, the fitting procedure proposed here is much more accurate.
422 The values of the coefficients are given in Table 3.

423 ***Table 3 : Values and errors of the fitting parameters of the K_2 equations as a function of Kn.***

$K_2 = (c_2Kn^2 + c_1Kn + c_0)^{-1}$	c_2	c_1	c_0	r^2
Value	$5.81.10^{-2}$	$5.55.10^{-3}$	$6.28.10^{-4}$	0.88432
Absolute standard error	$2.64.10^{-2}$	$1.80.10^{-3}$	$1.49.10^{-5}$	

424 For further calculations, considering $K_1 = C_1k_2$, where $C_1 = 1/(\Psi_s\varepsilon_{mf}^3) = 14$, according to Wen and Yu [36] and
425 $k_2 = 1.75$, according to Ergün [34] (the coefficient for the inertial regime), we get: $B = 1/K_1 = 0.0408$. For the
426 coefficient A, the equation of Re_{mf} as a function of Ar depends on the $K_2(Kn)$ parameter used for fitting. If we
427 consider $K_2 = (c_2Kn^2 + c_1Kn + c_0)^{-1}$, then we get:

$$Re_{mf} = \sqrt{\left[\frac{32.49}{1 + 8.83Kn + 92.56Kn^2}\right]^2 + 0.0408Ar} - \frac{32.49}{1 + 8.83Kn + 92.56Kn^2} \qquad \textit{Equation (14)}$$

428 *i.e.* a coefficient $A = 32.49/(1 + 8.83Kn + 92.56Kn^2)$, with an asymptotic value of 32.49 when Kn tends to 0.

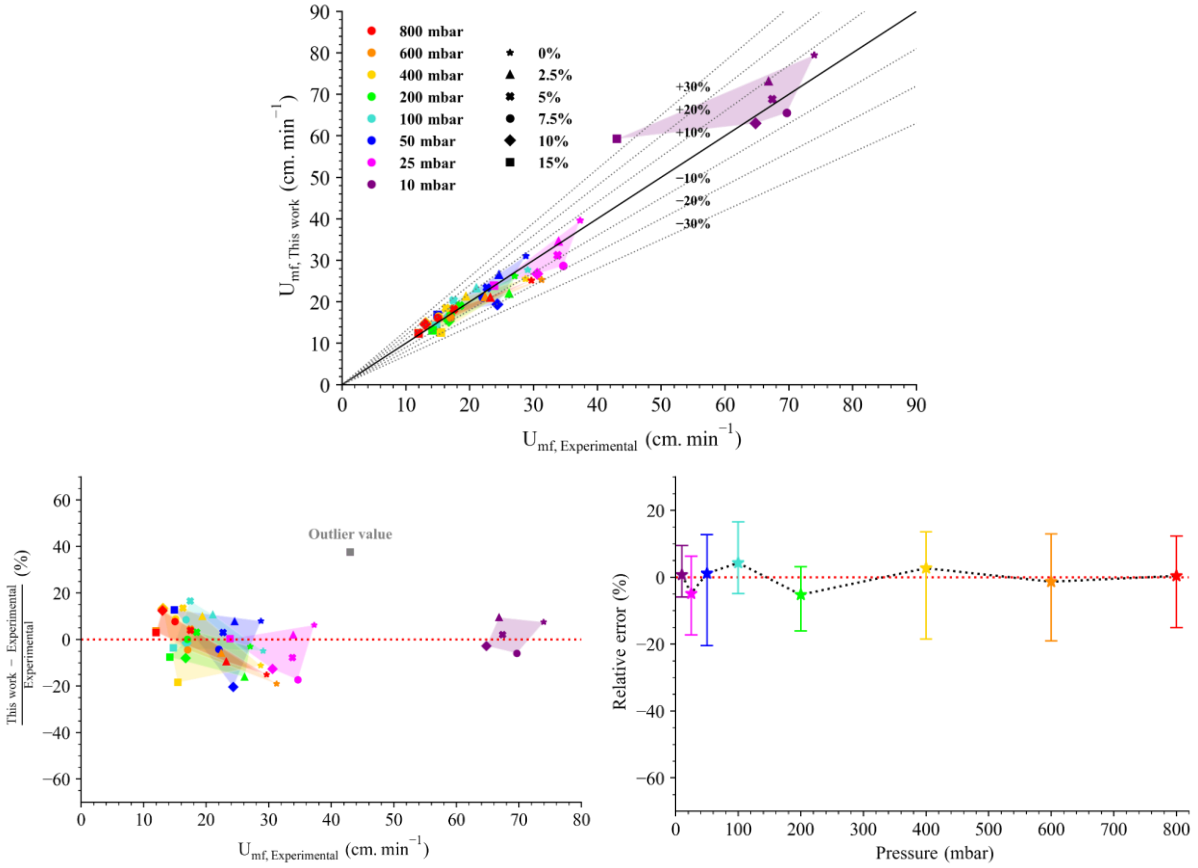

Fig. 16 : Comparison of minimum fluidization velocities from experiments and calculations with Equation (14) (top). Relative errors made by the calculation compared to the experimental values with Equation (14) (bottom left) and average errors with the minimum and maximum errors of the calculations with Equation (14) (bottom right) for each pressure.

Fig. 16 displays the comparison between the experimental data and the U_{mf} values calculated with Equation (14). The results are very satisfactory since the numerical prediction agrees with the experimental data, with an average absolute error of 8.3%. The point at 15% fiber mass fraction and 10 mbar (purple square point), which deviates from the prediction, seems to be an outlier. For all the other cases, the semi-empirical correlation with the inverse polynomial offers the best prediction for all fiber mass fractions.

5. Conclusion

Previous modeling studies have investigated the effect of adding short fibers to a powder load. This study proposes a description of the behavior of a bed composed of a mixture of short fibers and powder at variable ratios, and two semi-empirical correlations to describe the minimum fluidization velocity. It is obvious that short fibers, even when added in very small proportions, alter the hydrodynamic behavior of the mixture. With an elongated shape and a form factor greater than 10, these entities modify both the fluidization capacity of the

mixture and its intrinsic properties such as the porosity at minimum fluidization or the minimum fluidization velocity.

The present study investigates the effect of adding short fibers of micrometric dimensions to powders of the same chemical nature (SiC), also micrometric. Beyond a fiber mass fraction of 15%, fluidization becomes problematic at room temperature and reduced pressure. The charge tends to be cohesive and channeling occurs through a bed that becomes static. If an effective stirring is maintained for several tens of minutes it may stop for longer periods of time, the particles gradually agglomerating to form a static bed crossed by channels of preferential gas flow.

The minimum fluidization velocity was described by the Zarekar and Darcy-Klinkenberg equations. After a variable fitting parameter, it is possible to propose tortuosity constants and introduce an equivalent hydraulic diameter, which is itself fitted as a function of the proportion of short fibers. The modified Darcy-Klinkenberg equation correlates with the experimental data and provides an estimate of the minimum fluidization velocity with a mean absolute error of 14.9% and a standard deviation of 8.8%, compared to a mean absolute error of 18.2% and a standard deviation of 15.8% for the Zarekar equation. The discrepancy is even more pronounced at low working pressures, with a mean absolute error of 51.4% for the Zarekar equation and 12.3% for the Darcy-Klinkenberg equation.

The use of semi-empirical correlation has proven to be much more effective in describing U_{mf} as a function of the operating conditions. The values of the coefficients can be used and provide a prediction with an absolute error of less than 10% for all short fiber fractions in the mixtures. The numerical determination of this minimum fluidization velocity remains very important for the choice of fluidization operating conditions in the case of CVD coatings prepared at low pressures. This approach cannot be extended to other particles with other dimensions or aspect ratios, but it allows to propose a new methodology for determining U_{mf} with simple mathematical tools and little preliminary experimental work. It should be useful, for example, to select the flow rate of the gases injected into the reactor, to maximize the gas-solid exchange, a key parameter for the homogeneity of the coatings and the overall yield of the fluidized bed CVD process. These equations describing the fluidization behavior can also be integrated into a numerical simulation approach to model the fluidization of such unusual loads.

Acknowledgements

The authors are indebted to Sébastien Couthures and Rémi Bouvier for their contribution to the development and maintenance of the fluidized bed reactor. The University of Bordeaux is gratefully acknowledged for the grant to T. Da Calva Mouillevois as well as Safran Ceramics for the operational support and fruitful discussions.

Declaration of interests

The authors declare that they have no known competing financial interests or personal relationships that could have appeared to influence the work reported in this paper.

References

[1] Naslain R. Design, preparation and properties of non-oxide CMCs for application in engines and nuclear reactors: an overview. Compos Sci Technol 2004;64:155–70. https://doi.org/10.1016/S0266-3538(03)00230-6.

[2] Cavalier JC, Berdoyes I, Bouillon E. Composites in Aerospace Industry. Adv Sci Technol 2006;50:153–62. https://doi.org/10.4028/www.scientific.net/AST.50.153.

[3] Krenkel W. Ceramic Matrix Composites: Fiber Reinforced Ceramics and their Applications. 1. Aufl. Weinheim: Wiley-VCH; 2008.

[4] Naslain RR. The design of the fibre-matrix interfacial zone in ceramic matrix composites. Compos Part Appl Sci Manuf 1998;29:1145–55. https://doi.org/10.1016/S1359-835X(97)00128-0.

[5] Pompidou S, Lamon J. Une condition de déviation des fissures dans les CMC et les multicouches. Comptes Rendus Mécanique 2005;333:405–11. https://doi.org/10.1016/j.crme.2005.03.001.

[6] Weber GW, Beatty RL, Tennery VJ, Lackey WJ. The effect of pyrocarbon coating permeability on uranium redistribution in high temperature gas-cooled reactor fuels. Thin Solid Films 1977;40:123–30. https://doi.org/10.1016/0040-6090(77)90110-9.

[7] López-Honorato E, Tan J, Meadows PJ, Marsh G, Xiao P. TRISO coated fuel particles with enhanced SiC properties. J Nucl Mater 2009;392:219–24. https://doi.org/10.1016/j.jnucmat.2009.03.013.

[8] Liu R, Liu M, Chang J, Shao Y, Liu B. An improved design of TRISO particle with porous SiC inner layer by fluidized bed-chemical vapor deposition. J Nucl Mater 2015;467:917–26. https://doi.org/10.1016/j.jnucmat.2015.10.055.

[9] Salmasi A, Shams M, Chernoray V. An experimental approach to thermochemical conversion of a fuel particle in a fluidized bed. Appl Energy 2018;228:524–34. https://doi.org/10.1016/j.apenergy.2018.06.125.

[10] Liu B, Zhang X, Wang L, Hong H. Fluidization of non-spherical particles: Sphericity, Zingg factor and other fluidization parameters. Particuology 2008;6:125–9. https://doi.org/10.1016/j.cpart.2007.07.005.

[11] Oschmann T, Hold J, Kruggel-Emden H. Numerical investigation of mixing and orientation of non-spherical particles in a model type fluidized bed. Powder Technol 2014;258:304–23. https://doi.org/10.1016/j.powtec.2014.03.046.

[12] Nan W, Wang Y, Wang J. Numerical analysis on the fluidization dynamics of rodlike particles. Adv Powder Technol 2016;27:2265–76. https://doi.org/10.1016/j.apt.2016.08.015.

[13] Chen X, Zhong W, Heindel TJ. Fluidization of cylinder particles in a fluidized bed. Adv Powder Technol 2017;28:820–35. https://doi.org/10.1016/j.apt.2016.12.008.

[14] Mahajan VV, Padding JT, Nijssen TMJ, Buist KA, Kuipers J a. M. Nonspherical particles in a pseudo-2D fluidized bed: Experimental study. AIChE J 2018;64:1573–90. https://doi.org/10.1002/aic.16078.

[15] Nan W, Wang Y, Sun H. Experimental investigation on the packed bed of rodlike particles. Adv Powder Technol 2019;30:2541–7. https://doi.org/10.1016/j.apt.2019.07.034.

[16] Boer L, Buist KA, Deen NG, Padding JT, Kuipers JAM. Experimental study on orientation and de-mixing phenomena of elongated particles in gas-fluidized beds. Powder Technol 2018;329:332–44. https://doi.org/10.1016/j.powtec.2018.01.083.

[17] Geldart D, Harnby N, Wong AC. Fluidization of cohesive powders. Powder Technol 1984;37:25–37. https://doi.org/10.1016/0032-5910(84)80003-0.

[18] Kozulin NA. Mixing of powdered materials in a fluidized bed. Int Chem Eng 1965;5:157–61.

[19] Brekken RA, Lancaster EB, Wheelock TD. Fluidization of flour in a stirred aerated bed. Part II—solid mixing and circulation. Chem Eng Prog Symp Ser, vol. 66, 1970, p. 277–84.

[20] Wang S, Chen Y, Jia Y, Tian R, Sun Q, Fan J, et al. Numerical simulation of flow behavior of particles in a gas-solid stirred fluidized bed. Powder Technol 2018;338:119–28. https://doi.org/10.1016/j.powtec.2018.07.020.

[21] Chirone R, Massimilla L, Russo S. Bubble-free fluidization of a cohesive powder in an acoustic field. Chem Eng Sci 1993;48:41–52.

[22] Herrera CA, Levy EK, Ochs J. Characteristics of acoustic standing waves in fluidized beds. AIChE J 2002;48:503–13. https://doi.org/10.1002/aic.690480309.

[23] Cherntongchai P, Chaiwattana S, Leruk R, Panyaruean J, Sriboonnak S. Influence of standing wave characteristics on hydrodynamic behaviours in sound-assisted fluidization of Geldart group A powder. Powder Technol 2019;350:123–33. https://doi.org/10.1016/j.powtec.2019.01.031.

[24] Gao Q, Wang T, Tang T, He Y. Macroscopic and microscopic flow characteristics of particles in a sound assisted bubbling fluidized bed. Chem Eng Process - Process Intensif 2020;156:108102. https://doi.org/10.1016/j.cep.2020.108102.

[25] Valverde JM, Castellanos A, Quintanilla MAS. Effect of vibration on the stability of a gas-fluidized bed of fine powder. Phys Rev E 2001;64:021302. https://doi.org/10.1103/PhysRevE.64.021302.

[26] Luo Z, Fan M, Zhao Y, Tao X, Chen Q, Chen Z. Density-dependent separation of dry fine coal in a vibrated fluidized bed. Powder Technol 2008;187:119–23. https://doi.org/10.1016/j.powtec.2008.02.001.

[27] Stakić M, Urošević T. Experimental study and simulation of vibrated fluidized bed drying. Chem Eng Process Process Intensif 2011;50:428–37. https://doi.org/10.1016/j.cep.2011.02.006.

[28] Lehmann SE, Hartge E-U, Jongsma A, deLeeuw I-M, Innings F, Heinrich S. Fluidization characteristics of cohesive powders in vibrated fluidized bed drying at low vibration frequencies. Powder Technol 2019;357:54–63. https://doi.org/10.1016/j.powtec.2019.08.105.

[29] Jaraiz-M. E, Levenspiel O, Fitzgerald TJ. The uses of magnetic fields in the processing of solids. Chem Eng Sci 1983;38:107–14. https://doi.org/10.1016/0009-2509(83)80139-0.

[30] Arnaldos J, Casal J, Lucas A, Puigjaner L. Magnetically stabilized fluidization: modelling and application to mixtures. Powder Technol 1985;44:57–62. https://doi.org/10.1016/0032-5910(85)85021-X.

[31] Mori S. Vibro-fluidization of group-c particles and its industrial application. AIChE Symp Ser, vol. 86,

1990, p. 88–94.

[32] Dutta A, Dullea LV. A comparative evaluation of negatively and positively charged submicron particles as flow conditioners for a cohesive powder. AIChE Symp. Ser., vol. 86, 1990, p. 26–40.

[33] Da Calva Mouillevois T, Rivière C, Chollon G, Vignoles G, Bertrand N. Gaseous fluidization of short fibers and powders, influence of temperature and pressure. Chem Eng J 2023;453:139612. https://doi.org/10.1016/j.cej.2022.139612.

[34] Ergun S, Orning AA. Fluid Flow through Randomly Packed Columns and Fluidized Beds. Ind Eng Chem 1949;41:1179–84. https://doi.org/10.1021/ie50474a011.

[35] Zarekar S, Bück A, Jacob M, Tsotsas E. Reconsideration of the hydrodynamic behavior of fluidized beds operated under reduced pressure. Powder Technol 2016;287:169–76. https://doi.org/10.1016/j.powtec.2015.09.027.

[36] Wen CY, Yu YH. A generalized method for predicting the minimum fluidization velocity. AIChE J 1966;12:610–2. https://doi.org/10.1002/aic.690120343.

[37] Bourgeois P, Grenier P. The ratio of terminal velocity to minimum fluidising velocity for spherical particles. Can J Chem Eng 1968;46:325–8. https://doi.org/10.1002/cjce.5450460508.

[38] Saxena SC, Vogel GJ. The measurement of incipient fluidisation velocities in a bed of coarse dolomite at temperature and pressure. Meas Incipient Fluid Veloc Bed Coarse Dolomite Temp Press 1977.

[39] Babu S. P, Shah B, Talwalkar A. Fluidization correlations for coal gasification materials - Minimum fluidization velocity and fluidized bed expansion ratio. AIChE Symp Ser Am Inst Chem Eng 1978;74:176–86.

[40] Richardson JF, da S. Jerónimo MA. Velocity-voidage relations for sedimentation and fluidisation. Chem Eng Sci 1979;34:1419–22. https://doi.org/10.1016/0009-2509(79)85167-2.

[41] Thonglimp V, Hiquily N, Laguerie C. Vitesse minimale de fluidisation et expansion des couches fluidisées par un gaz. Powder Technol 1984;38:233–53.

[42] Chitester DC, Kornosky RM, Fan L-S, Danko JP. Characteristics of fluidization at high pressure. Chem Eng Sci 1984;39:253–61. https://doi.org/10.1016/0009-2509(84)80025-1.

[43] Tannous K, Hemati M, Laguerie C. Caractéristiques au minimum de fluidisation et expansion des couches fluidisées de particules de la catégorie D de Geldart. Powder Technol 1994;80:55–72. https://doi.org/10.1016/0032-5910(94)02841-9.

[44] Llop MF, Madrid F, Arnaldos J, Casal J. Fluidization at vacuum conditions. A generalized equation for the prediction of minimum fluidization velocity. Chem Eng Sci 1996;51:5149–57. https://doi.org/10.1016/S0009-2509(96)00351-X.

[45] Weerasiri LD, Das S, Fabijanic D, Yang W. Modelling the minimally fluidized state under reduced pressure. J Ind Eng Chem 2022;114:483–98. https://doi.org/10.1016/j.jiec.2022.07.038.

[46] Levenberg K. A method for the solution of certain non-linear problems in least squares. Q Appl Math 1944;2:164–8. https://doi.org/10.1090/qam/10666.

[47] Marquardt DW. An Algorithm for Least-Squares Estimation of Nonlinear Parameters. J Soc Ind Appl Math 1963;11:431–41. https://doi.org/10.1137/0111030.

[48] Feng R, Li J, Cheng Z, Yang X, Fang Y. Influence of particle size distribution on minimum fluidization velocity and bed expansion at elevated pressure. Powder Technol 2017;320:27–36. https://doi.org/10.1016/j.powtec.2017.07.024.

[49] Lewis WK, Gilliland ER, Bauer WC. Characteristics of Fluidized Particles. Ind Eng Chem 1949;41:1104–17. https://doi.org/10.1021/ie50474a004.

[50] Rashid TAB, Zhu L-T, Luo Z-H. Comparative analysis of numerically derived drag models for development of bed expansion ratio correlation in a bubbling fluidized bed. Adv Powder Technol 2020;31:2723–32. https://doi.org/10.1016/j.apt.2020.04.036.

[51] Wadell H. Volume, Shape, and Roundness of Rock Particles. J Geol 1932;40:443–51. https://doi.org/10.1086/623964.

[52] Charles C, Descamps C, Vignoles GL. Low pressure gas transfer in fibrous media with progressive infiltration: correlation between different transfer modes. Int J Heat Mass Transf 2022;182:121954. https://doi.org/10.1016/j.ijheatmasstransfer.2021.121954.

605 **Vitae**

Thomas Da Calva Mouillevois is a Ph.D. student in the development of ceramic coatings on short fibers by Fluidized Bed CVD process in the ThermoStructural Composites Laboratory since 2020. Graduated from the National Engineering School of Tarbes, France in the speciality of Structural Materials and Processes Engineering, Thomas Da Calva also holds a double degree in Materials Processing Characterization and Surface Treatments in partnership with the National School of Chemical and Technological Arts Engineers and the Paul Sabatier University of Toulouse.

Matthias Audren-Paul is an engineer in materials science graduated from ENSIACET (INP-Toulouse). He worked as an intern for 6 months on pyrolytic carbon and boron nitride coatings on short fiber and powder mixtures by FB-CVD in the ThermoStructural Composites Laboratory. He is also graduated from the University of Sherbrooke in nanomaterials and materials characterization.

Georges Chollon is research scientist at the French National Center for Scientific Research (CNRS) since 1999. He graduated from the National School of Physics and Chemistry of Bordeaux in 1990 and obtained a Ph.D. in Materials Science from the University of Bordeaux in 1995. He completed two post-doctoral fellowships, at EMPA-Dübendorf, Switzerland, in 1995-1996 and NIMCR-Tsukuba, Japan, in 1996-1998. At LCTS, he is investigating the relationships between synthesis (mainly by CVD), composition, structure and properties of carbon and non-oxide ceramics.

Nathalie Bertrand is an Assistant Professor in the Chemistry Department of the University of Bordeaux since 2003. She completed a Ph.D. in Chemical engineering in 2001 at Toulouse INP. Her main topics of interest concern Gaseous Fluidization, Transport phenomena and Chemical Vapor Deposition. Her current research activities focus on the use of Fluidized Bed-CVD process on short fibers.

606